**ASG**
SUPERCONDUCTORS

# MgB$_2$ OPENS THE DOOR TO HIGH PERFORMANCE MAGNET RAMPING

## Energy Storage, intraoperative MRI and particle therapy applications: empirical evidence shows MgB$_2$ confirms all theoretical expectations in carrying rapidly varying currents at 20K.

Alessio Capelluto and Lorenzo Mauro
*ASG Superconductors S.p.A., R&D division, Genova, Italy*

As is well known all types of superconductors are affected by AC losses.
Those losses occur when a time varying current flows in a superconductor or when it's subjected to a variable magnetic field. The main effect of these losses on the conductor is temperature rise due to the energy dissipation within the superconductor. Many methods were previously studied in order to reduce the magnitude of this loss. The main task of superconductor manufacturers is to optimize the design of the wire in order to reduce AC losses according to the magnet requirements.
This paper presents experiemenal results of an empiric experiment designed to demonstrate the theoretical benefit of MgB2, with respect to standard NbTi, in low-field/fast-ramped applications.

## 1 Introduction
## 1.1 AC losses

During current ramps the magnet wires are subjected to a variation of magnetic field. Superconductors subjected to varying magnetic fields see multiple heat sources that can impact on the conductor performance and stability. All the energy loss terms can be expressed as an equivalent magnetization loss induced in the conductor [1]. The superconductor $M - H$ cycle defines losses associated with magnetization: the area enclosed in a loop is lost as heat. This loss can be evaluated as

$$Q = \int \bar{M} \cdot d\bar{H} = \int \bar{H} \cdot d\bar{M} \qquad (1)$$

Two major contributions are taken in account: hysteresis losses and coupling losses. Using the simplest model [1] the equivalent magnetization linked to the first contribution is equal to:

$$M = \frac{2}{3\pi} J_c \, d_f \lambda \qquad (2)$$

Where $J_c$ is the critical current of the superconductor, $d_f$ is the diameter of the filaments that compose the wire and $\lambda$ is the ratio of the cross section areas of superconducting and resistive parts of the wire. It is possible to demonstrate that a superconducting wire subjected to an external varying magnetic field experiences an induced electric field which causes current to flow in the resistive wire stabilisation matrix. These induced currents are called inter-filament coupling current. In order to compare these losses to the hysteresis ones we can express the coupling losses as a magnetization contribution equal to [1]:

$$M = 2\dot{B}_i \tau \lambda_f \qquad (3)$$

where $\dot{B}_i$ is the time derivative of the internal magnetic field, $\tau$ is the raise time of the coupling currents and $\lambda_f$ is the fraction of the surface occupied by the superconducting filaments over the section of the entire wire. In conclusion, using this model, the power density generated during field variation is equal to:

$$P = \underbrace{\frac{2}{3\pi} J_c \, d_f \lambda \dot{B}_i}_{\text{hysteresis}} + \underbrace{2\tau\lambda_f \dot{B}_i{}^2}_{\text{coupling}} \qquad (4)$$

The parameters that most affect this heat generation are linked to the wire and strand geometry.

## 1.2 Temperature rise

A power loss inside a superconductor leads to a temperature rise. Depending on field amplitude and ramp speed this temperature rise can be high enough to cause transition to the normal state (quenching). Two main strategies can be used in order to reduce this phenomenon:

1. Wire and strand optimization
2. Increase of the enthalpy margin

Clearly those two methods can be combined in order to reduce the impact of AC losses on the performance of the wire.

The first method consists in optimising the manufacturing parameters of wire and strands in order to reduce the AC losses described in the previous section [2]. The second strategy is to reduce the temperature increase, not by reducing the losses, but by enlarging the enthalpy margin to transition of the conductor. To achieve this it is necessary to change materials and most importantly, to operate at high temperature. Indeed enthalpy has a strong dependence on the temperature:

$$H = \int_{Top}^{Tc} Cp\,(T)\,dT \; \alpha \; T^4 \tag{5}$$

Increasing the enthalpy margin leads to lower temperature rise with the same dissipated energy.
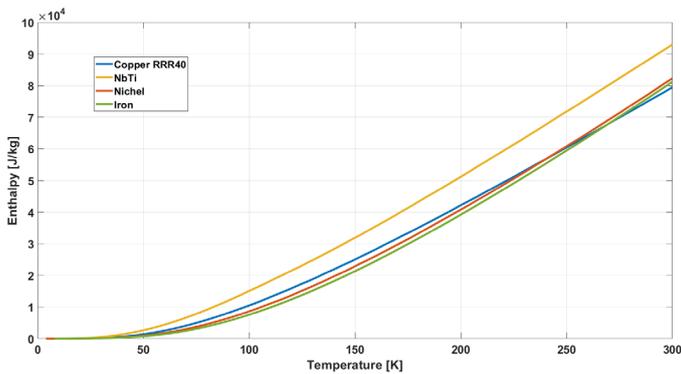


*Figure 1* Example of enthalpy for typical materials used in superconductor manufacturing

In the data analysis of this paper the enthalpy is replaced with the density of internal energy. This quantity can be evaluated using the simple relation:

$$E = \rho \cdot H \tag{6}$$

Where $E$ is the density of internal energy expressed in $J/m^3$ and $\rho$ is the density of the material taken in to account.

## 2 Empiric Experiment

An empiric experiment has been designed to compare the overall performance of NbTi and MgB$_2$ during field variation.

### 2.1 Design of the experiment

In order to compare NbTi and MgB$_2$ two solenoids were designed using legacy tool by ASG [5] and Cobham Opera [3].
The design was made using two standard commercial wires:

— NbTi commercial standard wire Ø1.8
— MgB$_2$ wire ASG MRO plus wire [4]

The results of the design are reported in the following list:

NbTi coil

— 1770 turns

— Ø 1.8 mm standard wire

($d_f$ *50 μm* / $l_p{}^1$ *50 mm*)

— Central field at 250$A$ = 1.4$T$

— Max field on conductor at 250A = 1.7$T$

— Inductance 0.77$H$

(without MgB$_2$ nickel matrix contribution effects)

MgB$_2$ coil

— 1768 turns

— 3.79 × 0.77 *mm* standard wire

($d_f$ *500 μm* / $l_p$ *750 mm*)

— Central field at 250$A$ = 1.4$T$

— Max field on conductor at 250A = 1.7$T$

— Inductance 0.75$H$

(without MgB$_2$ nickel matrix contribution effects)

The two coils have been designed to be as similar as possible from a magnetic point of view.
According to equation (4) greatest losses will be expected in the MgB$_2$ coil. In order to optimize and simplify the set up the two solenoids are wound on the same former as shown in *Figure 2*.

[1] $l_p$ is called twist pitch and is the axial length in which a filament or strand firstly returns to its original relative position in a twisted conductor. This parameter highly affects the AC performance of the wire.
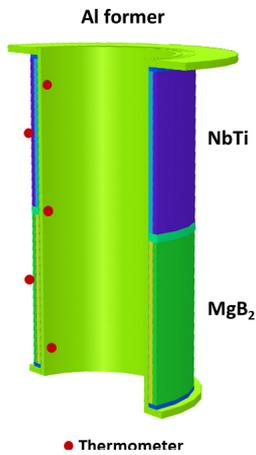
*Figure 2* Sketch of the experimental set up

The thermometers used in this experiment are the LakeShore Cernox CX-1050. The sensitivities of those sensors are shown in *Figure 3*. The typical sensor accuracy at *10K* is *± 6mK*.
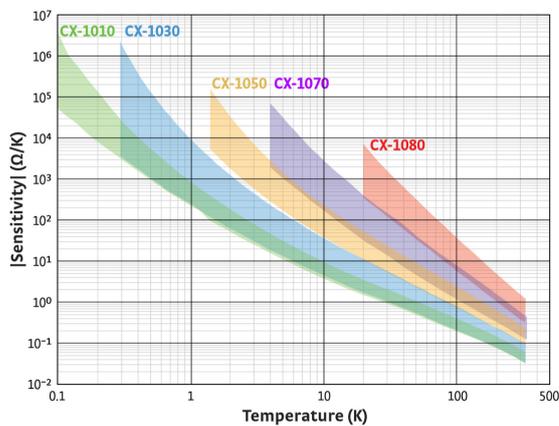


*Figure 3* Typical Cernox sensibility

## 2.2 Cooling system

The cryogenic system used to keep the set up cold is composed of a Sumitomo RDK 415D cryocooler and a Cryomech PT815 PulseTube. The cryocooler 2nd stage is linked to the NbTi side of the coil, while the 1st stage is used to keep the thermal shield cold. The PulseTube is used to refrigerate the current leads. The details of the cooling system are reported in *Table 1*.

|  | Dissipated heat [W] | Operating Temperature [K] |
|---|---|---|
| 1st stage RDK | 45 | 60 |
| 2nd stage RDK | 2 | 6 |
| 1st stage PT | 43 | 90 |
| 2nd stage PT | 12 | 15 |

*Table 1* Dissipated power and operating temperature of the different part of the set up (max field conditions)
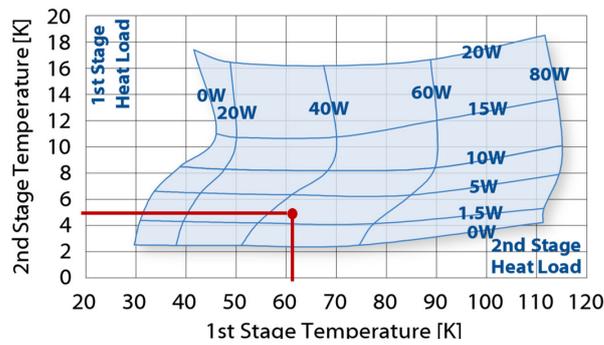


*Figure 4* Capacity map of Sumitomo RDK 415D and operating conditions of the facility (in red)

## 2.3 Electrical connection and bus bars

The two coils are connected in a three way system, as shown in *Figure 5*, but tested one at time. The power supply is capable of providing *6V* and *300A*.
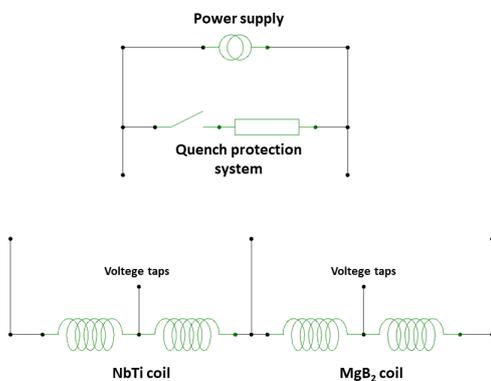


*Figure 5* Electrical scheme of the experimental set up

To reduce the heat input to the cold mass every lead is optimized in three different stages.
The protection system consists of an external dump resistor (2.3$\Omega$) and a quench detector with a *250ms/200mV* trigger. Those values are evaluated using the Cobham Opera [3] quench module. Using those values the tension during a quench will be lower than *300V* and the maximum temperature reached by the coil will be *120K* at *256A*, established to be the maximum allowable temperature for coil safety in the case of a quench.

## 2.4 Manufacturing process
A  6061 aluminium former is placed on the winding machine. Then two layers of glass tape, half overlapped, are installed as ground insulation. The volumes that will be occupied by the two coils are delimited using G10 curved profiles as shown in *Figure* 6.



*Figure* 6  Photo of the former placed on the winding machine with counter mass and G10 shoulders

The NbTi has the mid coil voltage tap placed at the 6th layer. The MgB$_2$ coil instead has the tap at the 13th layer. Once the wires are completely wound on the former another two layer of glass tape are wound over the magnet. To prevent any damage on the coil during the detachment of the extra epoxy resin after the impregnation one layer of PTFE tape is applied over the external counter mass. For the same reason all the surfaces are treated with a silicon based release liquid and all the brittle parts are covered with an appropriate soft filler. The result is shown in *Figure 7.*

*Figure 7* Photo of the coil before the impregnation process

The impregnation is made using an epoxy resin compatible with the materials used and the autoclave setting at 110°C for 96 hours. After impregnation and cleaning of the coil is set in position.

## 2.5 Final assembly

The coil is held in place using eight threaded rods (Ø6$mm$, L250$mm$) made of fiberglass N. Those rods are hung from the thermal shield in order to reduce the thermal input to the cold mass. The thermal link between the 2$^{nd}$ stage of the cryocooler and the coil is made with twelve 5N aluminium bars (20×4×250 $mm^3$). The shield is made of aluminium covered with 30 layers of MLI and kept in place by three threaded rods (Ø8$mm$, L350$mm$) made of fiberglass N linked to the vacuum chamber upper flange.



*Figure 8* Photo of the facility before the closure of the vacuum chamber

The connection between the 1$^{st}$ stage of the RDK and the shield is achieved using eight copper braid of 25 $mm^2$ section and 300 $mm$ length. The cold mass, thermal shield, current leads and the two cold heads are linked to the upper flange of the vacuum chamber.

## 3 Experimental Data

As first several voltage controlled ramps have been done in order to caracterize the coil responses to fast charges up to the faster one in a fixed current range of *100A*. The MgB$_2$ winding presents higher inductance, than calculated from theory, believed to be due to to the nickel matrix. This implies that ramp speed would be slower than NbTi at the same voltage.

After checking compatibility of the system with the maximum voltage of *6V* all the further ramps are done at the highes ramp speed. In the NbTi coil at max ramp speed, at *130A*, the quech protection system detects a resistive transition: the NbTi reached somewhere the critical tempereture. On the other side the MgB$_2$ coil reached, without thermal drawbacks, a current of *256A* at maximum ramp speed. Relaxing the maximum acceptable quench temperature, it would be possible to reach higher current at the same ramp up rate.
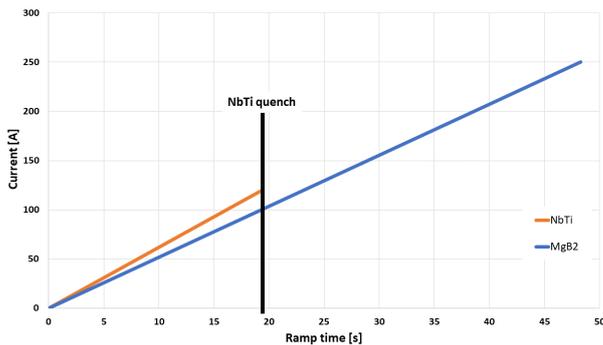


*Figure 9* Recorder current during maximum speed ramp

From the recorded *100A* ramps data is possible to evaluate the following results:

| P.S. output Voltage [V] | Current Increase [A] | Temperature Increase   [K] | Ramp time [s] | Ramp rate [A/s] | Estimated energy release [$J/m^3$] |
|---|---|---|---|---|---|
| 1.5 | 100 | 0.39 | 64 | 1.56 | 2431 |
| 2 | 100 | 0.22 | 48 | 2.08 | 3230 |
| 3 | 100 | 0.45 | 37 | 2.70 | 6594 |
| 5 | 100 | 0.57 | 26 | 3.85 | 8361 |
| 6 | 100 | 0.74 | 19 | 5.26 | 10831 |

*Table 2* A selection of ramp up data of MgB$_2$ winding

| P.S. output Voltage [V] | Current Increase [A] | Temperature Increase [K] | Ramp time [s] | Ramp rate [A/s] | Estimated energy release [$J/m^3$] |
|---|---|---|---|---|---|
| 1.5 | 100 | 0.35 | 57 | 1.75 | 1357 |
| 2 | 100 | 0.47 | 46 | 2.17 | 1832 |
| 2.5 | 100 | 0.58 | 40 | 2.50 | 2262 |
| 3.5 | 100 | 0.83 | 27 | 3.70 | 3236 |
| 6 | 100 | 1.32 | 16 | 6.25 | 5147 |

*Table 3* A selection of ramp up data of NbTi winding

As shown in *Table 2* and T*able 3* the ramps are fast enough to be considered adiabatic and the temperature increases are low enough to allow evaluation of the density of the released energy as follow:

$$E = \rho \cdot Cp \cdot \Delta T - E_{eddy} \qquad (7)$$

Where $\rho$ is the winding density, $Cp$ is the specific heat capacity and $\Delta T$ is the temperature increase during ramp up. $E_{eddy}$ is the contribution to the temperature increase due to the eddy current induced in the aluminium former. This contribution is evaluated using the Elektra Transient module of Opera [3]. The calculation of the $Cp$ of the wires is done by making a weighted average of the materials that compose them. The wire compositions are shown in *Figure 10*. The bulk heat capacity calculation takes into account also the insulation physical properties.

### MgB$_2$ wire
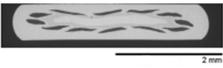


| Material | Area [$mm^2$] | % |
|---|---|---|
| Nichel | 1.39 | 63 |
| Copper | 0.33 | 15 |
| MgB$_2$ | 0.26 | 12 |
| Iron | 0.22 | 10 |
| **Total** | **2.20** | **100** |

### NbTi wire
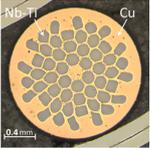


| Material | Area [$mm^2$] | % |
|---|---|---|
| Copper | 2.03 | 88 |
| NbTi | 0.29 | 12 |
| **Total** | **2.32** | **100** |

*Figure 10* Detail of the composition of wires

As expected the energy released during ramps is higher in the MgB$_2$ winding as shown in *Figure 11*, but the overall performance is better.
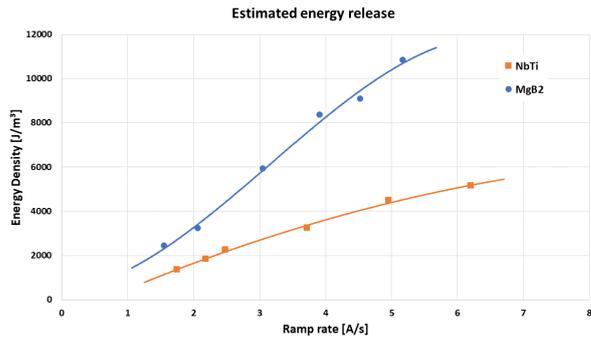
*Figure 11*  Energy release at different ramp rate

The higher energy margin compensates for the higher losses. Indeed, as is shown in *Figure 12* and *Figure 13*, the MgB$_2$ energy needed to reach the normal state is 40 – 100 times higher than for the NbTi.
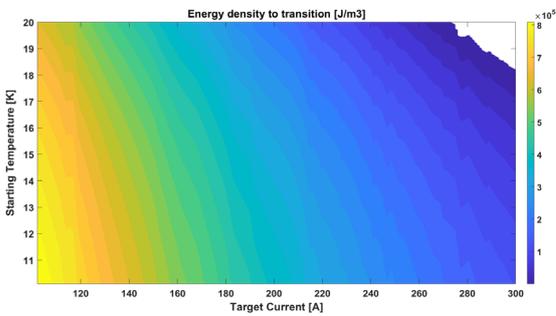


*Figure 12*  Energy density to transition for MgB$_2$ winding as function of starting temperature and target current (adiabatic conditions)
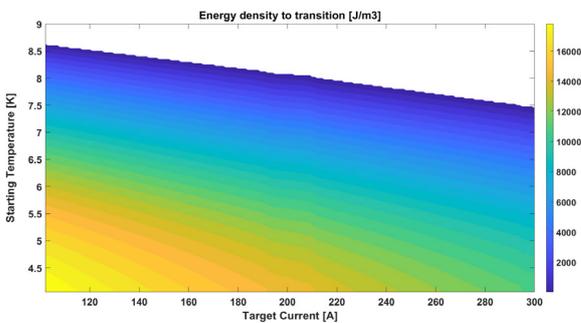


*Figure 13*  Energy density to transition for NbTi winding as function of starting temperature and target current (adiabatic conditions)

The density of energy to transition shown in the two previous figures was evaluated using the relation:

$$\mathrm{E} = \rho \cdot \int_{Ts}^{Tc\,(I,B)} Cp\,(T) \cdot dT \qquad\qquad (8)$$

www.asgsuperconductors.com

Where $T_S$ is the starting temperature of the magnet and $T_C$ (I,B) is the critical temperature of the superconductor as a function of operating current and external field. Some values of critical temperature are shown in *Figure 14* and *Figure 15*.
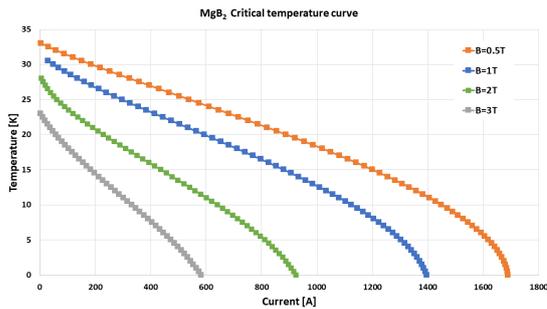


Figure 14  Critical temperature curve of MgB$_2$ MRO plus wire
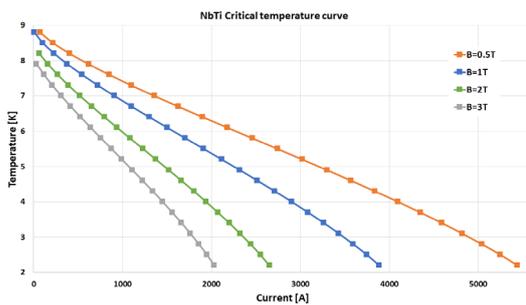


*Figure 15*  Critical temperature curve of NbTi standard Ø1.8

## 4 Conclusions

As empirically demonstated by the previous data operating at higher temperature naturally means a wire more resiliant to field variations. Indeed the enthalpy benefits are neglible at low temperature because of the temperature dependance ($H \, \alpha \, T^4$). As can be deduced from *Figure 12* and *Figure 13* reducing the operating temperature of the MgB$_2$ coil from $15K$ to $14K$ increases the energy margin by 35 times more than in the case of the same temperature decrease of $1K$ at $5.2K$ for the NbTi coil.

## 4.1 Clarification example

To clarify the difference between temperature and energy margin an example, based on the measured data, will follow. Consider two coils, like those used for the experiment, ramped in 80 seconds up to $2T$. In *Table 4* the energy densities released during the ramp up are shown.

| Energy density released in 80s ramp to *2T* for NbTi | Energy density released in 80s ramp to *2T* for MgB2 |
|---|---|
| 9380 $J/m^3$ | 24000 $J/m^3$ |

*Table 4* Energy density released during ramp up of NbTi and MgB2 windings

As shown in *Figure 16* the energy released during the ramp up will bring the magnet to the transition temperature even if the starting temperature is 5.2$K$ or 4.2$K$. In this case a 1$K$ margin gives only a 900 $J/m^3$ energy margin. This implies that in these conditions the temperature margin doesn't pratically affect the final temperature.
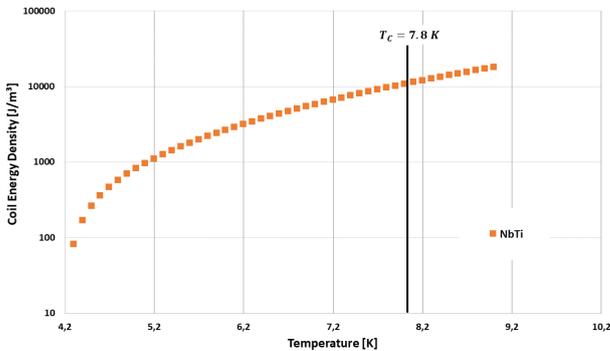


*Figure 16* NbTi coil energy density as function of temperature

On the other side the MgB2 winding release more energy, during ramp up, due to the wire architecture. However the energy margin to transition is many times bigger because of the higher operating temperature. The same starting temperature difference of 1$K$ leads to different final temperature as shown in *Figure 17*.
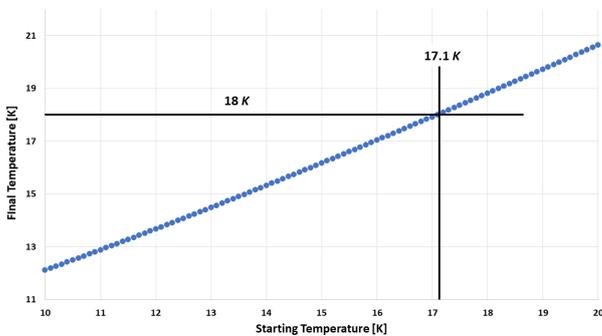


*Figure 17* Relation between starting and final temperature of the MgB2 winding during ramp up

## 4.2 AC losses optimization

Neither wires were optimized for AC losses but the MgB$_2$ demonstrated to be more adapt for low-field/fast-ramped applications than a standard NbTi wire. ASG MgB$_2$ wire division is improving the manufacturing process to optimize the wire parameters for AC losses. The state of art of AC losses optimization for MgB$_2$ wire is shown and compared to the wire used in this experiment in *Table 5*.

| Used for this experiement | | State of art | |
|---|---|---|---|
| $d_f$ [$\mu m$] | $l_p$ [$mm$] | $d_f$ [$\mu m$] | $l_p$ [$mm$] |
| 500 | 750 | 55 | 85 |

*Table 5* Comparison between sate of art of MgB2 wire and the one used for this experiment

Another pro of higher operating temperature is the costs reduction of the cryogenics. Indeed, using a cryocooler cooling system, a typical refrigerating power of $13W$ at $15K$ costs one half of a refrigerating power of $1.5W$ at $4.2K$.

## 4.3 Consecutive ramps

All the presented results are refered to a single ramp, fast enough to be considered adiabatic. During this experiment some consecutive ramps are recorded in order to emirically evaluate the overall response of the system. The aim of this paper is not to analize the behaviour of consecutive ramps. More complex studyes will be done taking in account the thermal diffusivity and all the non-neglible effects of consecutive charges.

The recorded data are resumed in the following graph.
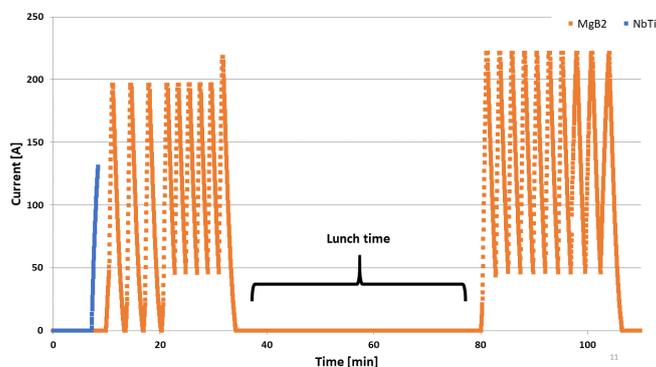


*Figure 18* Recorded current during multiple ramp up

As it's possible to see in *Figure 18*, the MgB$_2$ coil does not reach the operational critical value despite repeated charges and discharges in different current ranges.

**References**
[1] Wilson Martin N. 1983 *Superconductin Magnets* Oxford Science Pubblication

[2] M. Lyly, M. Holm, A. Stenvall and R. Mikkonen, *Design Process for a NbTi Wire With New Specification Objectives: Technical Design Constraints and Optimization of a Wire Layout Considering Critical Current and AC Losses*, in IEEE Transactions on Applied Superconductivity, vol. 23, no. 1, pp. 6000910-6000910, Feb. 2013, Art no. 6000910, doi: 10.1109/TASC.2012.2232918.

[3] Dassault Systemes *Opera version* 14R1 x64, www.3ds.com, 2018.

[4] ASG Superconductors S.p.A. Wire for MRI systems PLUS, www.asgsuperconductors.com

[5] A. Capelluto, M. Nervi, P. Molfino, 2014. *Algorithm for the Fast Calculation of Magnetic Fields Generated by Arc-Shaped Conductors With Rectangular Cross Section.* IEEE Transactions on Applied Superconductivity. 24. 1-5. 10.1109/TASC.2014.2326918.